JMEPEG (2019) 28:567–577
https://doi.org/10.1007/s11665-018-3777-9

1059-9495/$19.00

Impact of Hot Bending on the High-Temperature Performance and Hydrogen Damage of 2.25Cr-1Mo-0.25V Steel

Song Huang, Zhiping Chen, You Li, and Delin Zhang

(Submitted March 26, 2018; in revised form August 13, 2018; published online December 6, 2018)

The impact of hot bending forming process on the high-temperature mechanical properties and hydrogen damage of 2.25Cr-1Mo-0.25V steel was investigated by scanning electron microscope (SEM), transmission electron microscope (TEM), energy-dispersive spectrum (EDS) and the slow strain rate tensile (SSRT) test in high-temperature hydrogen environment. The samples containing hot bending residual influence were extracted from a real hydrogenation reactor shell fabricated through hot bending–welding process. SEM images of the material demonstrated that the density and size of carbides in 2.25Cr-1Mo-0.25V increased after forming. TEM and EDS results revealed that ferrite matrix of the formed material was purified. The mechanical properties measured by SSRT test manifested that 2.25Cr-1Mo-0.25V was softened after forming. Moreover, it was observed that high-temperature hydrogen environment embrittled the material and the susceptibility to hydrogen damage increased after forming. The role of hot bending process on the evolution of mechanical properties and hydrogen damage susceptibility was discussed. Possible mechanism for the impact of hot bending process on the high-temperature hydrogen damage was proposed.

Keywords high-temperature property, hot bending forming, hydrogen damage, hydrogenation reactor, manufacturing residual influence, 2.25Cr-1Mo-0.25V

1. Introduction

2.25Cr-1Mo-0.25V steel is a largely used structural material for hydrogenation reactor owing to its excellent resistance against high-temperature creeping and hydrogen attack (HA). As an upgraded version of 2.25Cr-1Mo steel, 2.25Cr-1Mo-0.25V steel possesses the advantages of higher strength and higher allowable temperature, which is attractive for the popular trend of lightweight design.

In the fabrication of a hydrogenation reactor, considerable energy will be embraced into the raw material during the manufacturing processes such as heat treatment, plastic forming and welding, which could leave permanent influences on the performance of a product (Ref 1). A typical example of manufacturing residual influence was reported by Zeng et al. (Ref 2), which reported that the results of car crash simulation with manufacturing-induced material properties matched well with the experimental results while the simulation with nominal properties failed to predict the failure of car. Therefore, the conventional concept of safety factor cannot guarantee the safety of equipment as the manufacturing residual influence cannot be ignored. On the other hand, physical property such as hydrogen diffusivity (Ref 3) of material could be influenced by manufacturing processes. Wang et al. (Ref 4) also reported that the high-temperature plastic deformation (HTPD) at 660 °C increased the hydrogen embrittlement susceptibility of 2.25Cr-1Mo-0.25V steel. Therefore, manufacturing residual influence should be considered as a potential risk in the design process of hydrogen-related equipment such as hydrogenation reactor. In order to close the gap between realistic products and engineering design methodologies, it's necessary to pursuit further understanding of the impact of manufacturing residual influence on the material performance.

Hydrogenation reactor is a thick-walled pressure vessel whose shell is fabricated through hot bending–welding or hot forging–welding process. The hot bending process (HBP) for a 2.25Cr-1Mo-0.25V made hydrogenation reactor shell is conducted under 650-675 °C, which brings both tempering effect and plastic deformation to the material simultaneously. Recently, studies (Ref 4-7) have manifested that HBP could have changed the room temperature properties of the structural material before hydrogenation reactor began its service. Nevertheless, hydrogenation reactor serves at temperature above 400 °C, where the material behaves differently with that at room temperature. Therefore, it's essential to investigate the impact of manufacturing processes on the high-temperature properties of 2.25Cr-1Mo-0.25V steel, especially when corrosive hydrogen environment is involved in. But to the best knowledge of the authors, related study has not been reported yet.

The purpose of this paper is to investigate the impact of hot bending forming process on the mechanical properties and hydrogen damage of 2.25Cr-1Mo-0.25V steel at high temperature. The slow strain rate tensile (SSRT) test of the material with or without the HBP residual influence will be conducted in high-temperature hydrogen environment. Then the evolution of mechanical properties and microstructure will be investigated. The present work will contribute to the further understanding of

Song Huang, Zhiping Chen, You Li, and **Delin Zhang**, Institute of Process Equipment, Zhejiang University, 38 Zheda Road, Hangzhou 310027 Zhejiang, People's Republic of China. Contact e-mail: zhiping@zju.edu.cn.

the impact of manufacturing processes on the safety of hydrogen-related equipment.

2. Experimental Method

2.1 Material Preparation

The 2.25Cr-1Mo-0.25V steel for the SSRT test was received in the form of thick plate with 152 mm in thickness. The as-received steel was normalized in 930 °C and tempered in 720 °C. Chemical compositions of the material are listed in Table 1, which shows that the material meets the composition requirement in ASME standard. A part of the as-received plate had been hot-bended into a cylindrical ring at 650 °C to generate HBP residual influence. The resulting cylindrical ring with inner diameter D_i = 2400 mm and thickness t = 152 mm is shown in Fig. 1(a). The hot forming process applied here is a realistic fabrication process for hydrogenation reactor, where the raw plate was firstly heated into 650 °C and then bended into cylinder with a single forming pass and several correction passes.

The samples were removed from both outside surface and center of the cylindrical ring as well as the as-received plate. The sampling location is illustrated in Fig. 1(b). Tensile samples with a gauge of $\phi 5 \times 25$ mm were prepared. In the rest of the present work, the samples obtained from surface of the as-received plate are referred as as-received (AR) samples, the samples from center of the plate are referred as as-received-center (ARC) samples, the samples from surface of the formed cylindrical ring are referred as after-forming (AF) samples, and the samples from center of the cylindrical ring are referred as after-forming-center (AFC) samples.

2.2 Slow Strain Rate Tensile Test

SSRT test was carried out on the material testing apparatus in Hefei General Machinery Research Institute, P.R. China. The testing apparatus allows the test in 1 MPa pressurized hydrogen environment with temperature up to 600 °C, and the details of parameters in this apparatus can be found in Ref 8. The atmosphere used in the present work was hydrogen (H_2) and argon (Ar) with purity of 99.999%. Three cases were considered. In Case1, the SSRT test was implemented in 510 °C + 1 MPa argon environment as control group. All four groups of samples (AR, AF, ARC and AFC) were tested in Case1 to investigate the HBP residual influence in the absent of hydrogen. Case2 was carried out in 510 °C + 1 MPa hydrogen environment. In Case3, the samples were immersed into 510 °C + 1 MPa hydrogen environment without loading for 24 h to pre-charge hydrogen and then tested immediately. For Case2 and Case3, only AR samples and AF samples were tested. The reason is that the surface of cylindrical ring has the most pronounced residual influence due to the plastic deformation. The test temperature 510 °C was chosen based on the highest allowable temperature of 2.25Cr-1Mo-0.25V steel restricted by the Nelson curve in API 941 (Ref 9). The strain rate for SSRT test was 4×10^{-5}/s corresponding to a loading rate of 0.06 mm/min. Details about the experimental conditions and the mark of samples are listed in Table 2.

Table 1 Chemical composition of the experimental material (wt.%)

Element	Standard	Experimental material
C	≤ 0.17	0.12
Cr	2.0-2.5	2.4
Mo	0.9-1.1	0.99
V	0.25-0.35	0.32
Ni	≤ 0.25	0.11
Mn	0.3-0.6	0.55
Si	≤ 0.10	0.05
P	≤ 0.015	0.002
S	≤ 0.010	0.001

2.3 Microstructure Observation

The microstructure and fracture surface of the samples were investigated by optical microscope (OM), scanning electron microscope (SEM, Hitachi SU-70) and transmission electron microscope (TEM, Tecnai G2 F20 S-TWIN) equipped with energy-dispersive spectrum (EDS). 4% Nital was used to reveal the microstructure.

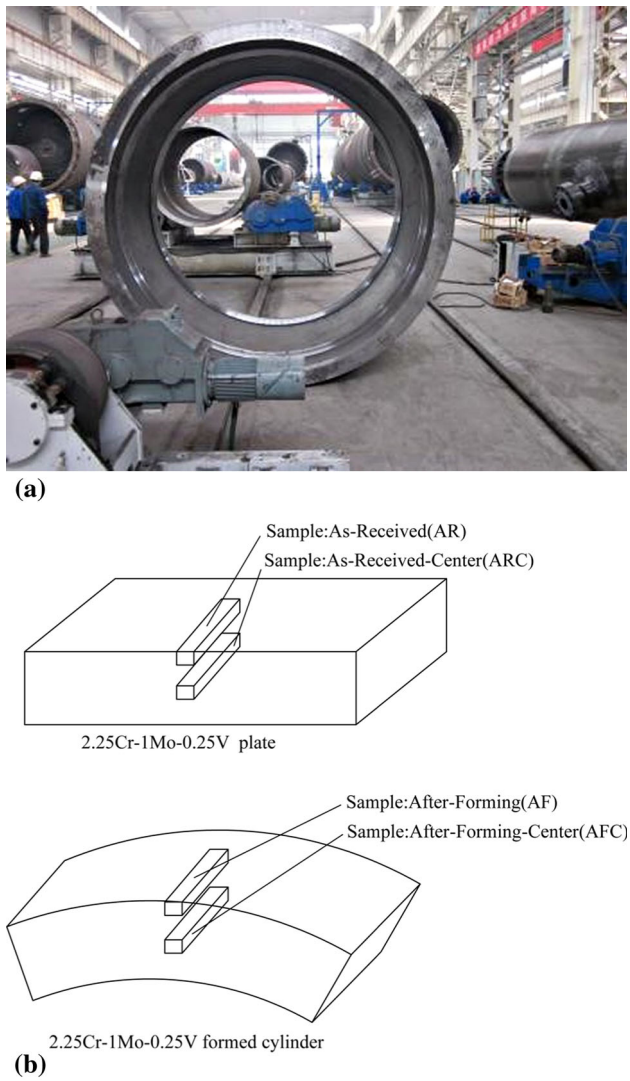

Fig. 1 Test sample preparation: (a) formed cylinder; (b) sampling location

Table 2 Experimental conditions

Cases	Sample mark	Material	Experimental condition
Case 1	AR-Ar	AR	510 °C + 1 MPa Ar
	AF-Ar	AF	510 °C + 1 MPa Ar
	ARC-Ar	ARC	510 °C + 1 MPa Ar
	AFC-Ar	AFC	510 °C + 1 MPa Ar
Case 2	AR-H2	AR	510 °C + 1 MPa H_2
	AF-H2	AF	510 °C + 1 MPa H_2
Case 3	AR-H2-24	AR	510 °C + 1 MPa H_2 pre-charge 24 h
	AF-H2-24	AF	510 °C + 1 MPa H_2 pre-charge 24 h

2.4 Microstructure Statistics

Image analysis technique was employed to study the evolution of carbides in microstructure. The statistic process was implemented as follows: The SEM images of the microstructure were firstly transformed into grayscale map. Then the light objects in the image (i.e., carbides) were selected by the OpenCV software. At last, the size and amount of selected objects were counted by Image-Pro software.

3. Experimental Results

In the present work, the nominal yield strength corresponding to 0.2% plastic strain (YS), the ultimate tensile strength (UTS), the elongation and the area reduction ratio were measured. The results of Case1 are shown in Fig. 2. The results of SSRT in hydrogen environment are shown in Fig. 3. The resulting engineering stress–plastic strain curves of AR and AF samples in Case1–Case3 are shown in Fig. 4.

3.1 High-Temperature Mechanical Properties

In Case1, for the samples from the surface of plate and cylinder (i.e., AR samples and AF samples), the YS reduced from 436 to 359 MPa after HBP, presenting a strength loss of 17.7%. Compared with the UTS of AR sample (476 MPa), the UTS of AF sample (418 MPa) reduced about 12.2%. Meanwhile, HBP increased the elongation from 19.2 to 21.7% and area reduction changed slightly from 86.5 to 88.2%. It is concluded that HBP resulted in the strength reduction as well as ductility increase at high temperature. In other words, 2.25Cr-1Mo-0.25V steel was softened after HBP.

In Fig. 2, one can also find that the mechanical properties of ARC and AR samples are identical, indicating the as-received plate is homogeneous from surface to center. However, the results of AFC and AF samples demonstrate that the strength of AF sample is lower than AFC sample, which means the surface of cylinder suffered more softening than the center of cylinder. The inhomogeneous softening in the cylinder implies that the high-temperature plastic deformation during HBP is the driving force of HBP residual influence.

3.2 High-Temperature Hydrogen Damage

Given the fact that AR-H2-24 & AF-H2-24 samples were immersed in 1 MPa hydrogen environment for 24 h, then it is reasonable to consider that hydrogen concentration in Case3 is higher than that in Case2. Such the intensity of hydrogen's effect on the samples is sorted as Case1 < Case2 < Case3.

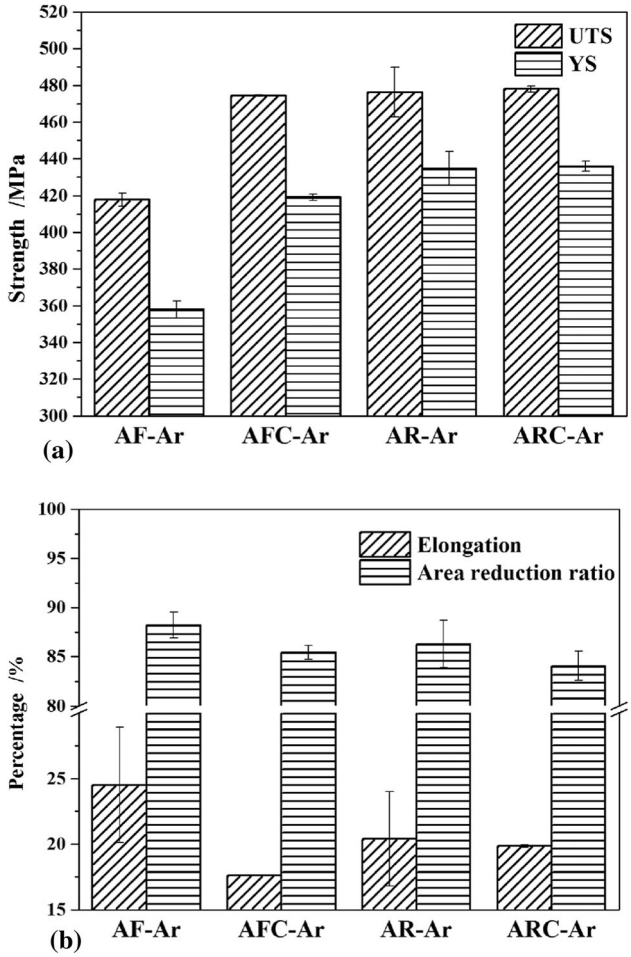

Fig. 2 Experimental results of Case1: (a) yield strength and ultimate tensile strength; (b) elongation and area reduction

Hydrogen's effect on the tensile strength is displayed in Fig. 3(a), which demonstrates that high-temperature hydrogen has inappreciable effect on the strength of AR material. However, the YS and UTS of AF material increased in the presence of hydrogen. Comparison between the results of AR material and AF material manifests that hydrogen has more significant influence on the strength of AF material.

In Fig. 3(b), ductility loss represented by the reduction in elongation can be identified for both AR and AF material, while no apparent difference is found in the results of area reduction.

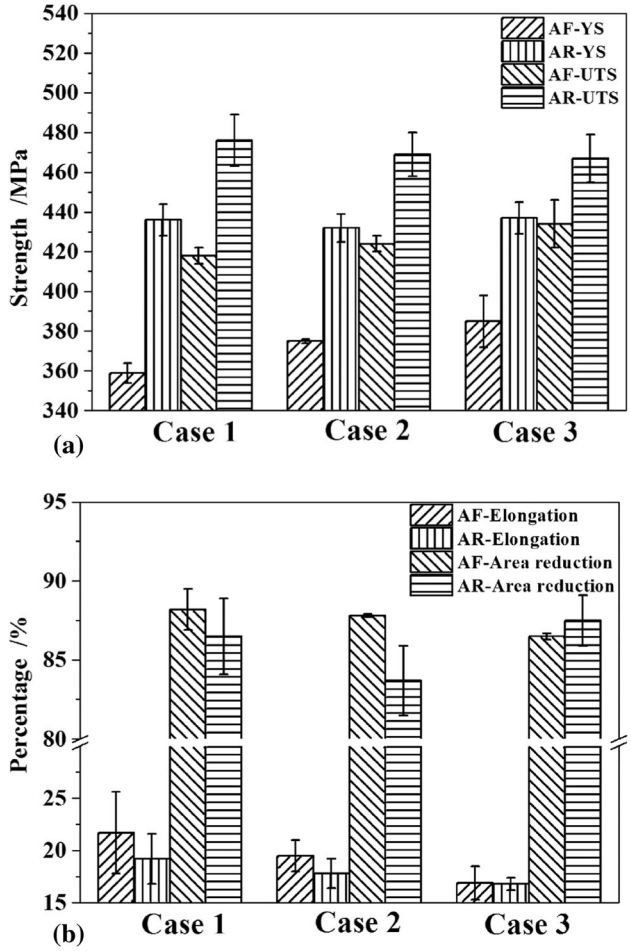

Fig. 3 Experimental results of SSRT in hydrogen environment: (a) yield strength and ultimate tensile strength; (b) elongation and area reduction

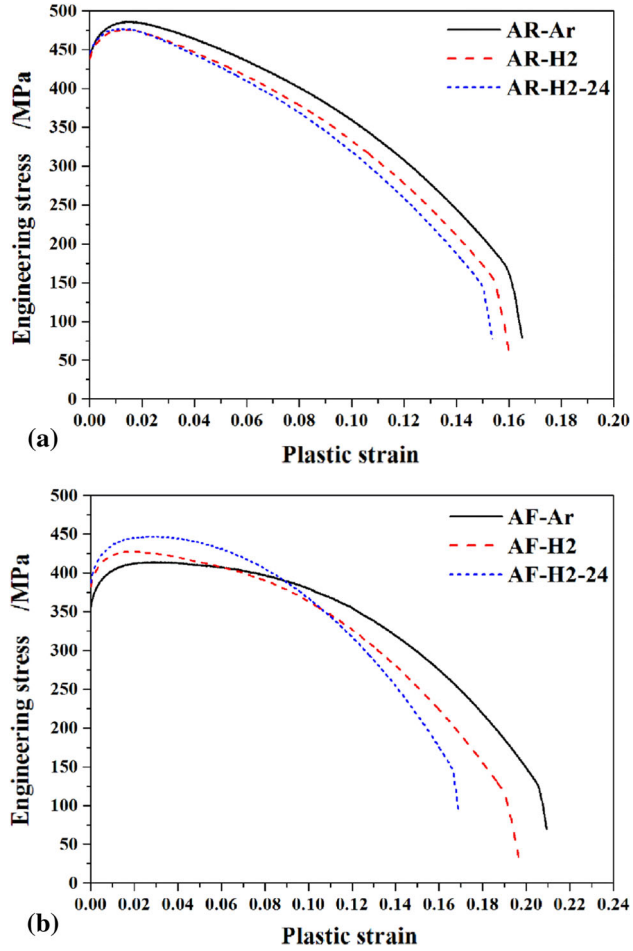

Fig. 4 Engineering stress–plastic strain curve: (a) as-received samples; (b) after-forming samples

Hydrogen damage susceptibility factor δ_H is defined as (Ref 10):

$$\delta_{\mathrm{H}} = \frac{\varepsilon - \varepsilon_{\mathrm{H}}}{\varepsilon} \times 100\% \qquad \text{(Eq 1)}$$

where ε and ε_{H} are the elongation without and with hydrogen's effect. The δ_{H} of all hydrogen-involved samples is listed in Table 3. As is demonstrated in Table 3, hydrogen pre-charge increased the δ_{H} of AR samples from 7.3% (AR-H2) to 12.5% (AR-H2-24), which is an increment of 5.2%. Meanwhile, for AF material, δ_{H} increased 12% from 10.1% (AF-H2) to 22.1% (AF-H2-24) after hydrogen pre-charge. AF material exhibits more susceptibility to hydrogen-induced embrittlement in both Case2 and Case3. With the elevation of hydrogen concentration in material, AF material presents more δ_{H} elevation than AR material. The results indicate that HBP residual influence enhanced the hydrogen damage susceptibility of 2.25Cr-1Mo-0.25V steel at high temperature. Same conclusion can also be drawn from the stress–strain curves shown in Fig. 4(a) and (b).

3.3 Microstructure

Figure 5 shows the OM images of AR material and AF material. It is shown that the microstructure of 2.25Cr-1Mo-0.25V steel is granular bainite with a composition of ferrite matrix (light phase in OM image) and retained M/A phase (brown phase in OM image). According to Fig. 5(a), the average grain size is approximated as 10-15 μm. The microstructure of AF material is shown in Fig. 5(b), which exhibits that the ferrite grains have deformed due to HBP. Besides, the retained M/A phase in AF material has decomposed further compared with AR material, which means the high-temperature tempering should contribute to the softening after HBP.

SEM images of the materials are shown in Fig. 6. The statistical results of the carbides are shown in Fig. 7. The carbide statistics of each material are based on 10 SEM images with × 10,000 magnification. It is found that all the microstructures have dispersed tiny carbides and several coarse large carbides. The carbide statistics shown in Fig. 7 demonstrates that AF & AFC samples possess more carbides than AR & ARC samples. Besides, the tiny carbides decorated on the ferrite tends to be coarsening after HBP. It is also demonstrated that the carbide density in AR and ARC samples are similar while carbide density in AF samples are obviously higher than that in AFC samples, which could be related with the effect of high-temperature plastic deformation.

TEM images of AR and AF samples (before test) are shown in Fig. 8(a). The EDS mappings of C, Cr, Mn, V, Mo elements for the TEM images are given. The element analysis results on the ferrite matrix [boxes in Fig. 8(a) and (b)] are also demonstrated in the images. For AR sample shown in Fig. 8(a),

Table 3 Hydrogen susceptibility factor

Cases	Sample mark	Experimental condition	δ_H, %
Case2	AR-H2	510 °C + AR + 1 MPa H_2	7.3
	AF-H2	510 °C + AF + 1 MPa H_2	10.1
Case3	AR-H2-24	510 °C + AR + 1 MPa H_2 pre-charge 24 h	12.5
	AF-H2-24	510 °C + AF + 1 MPa H_2 pre-charge 24 h	22.1

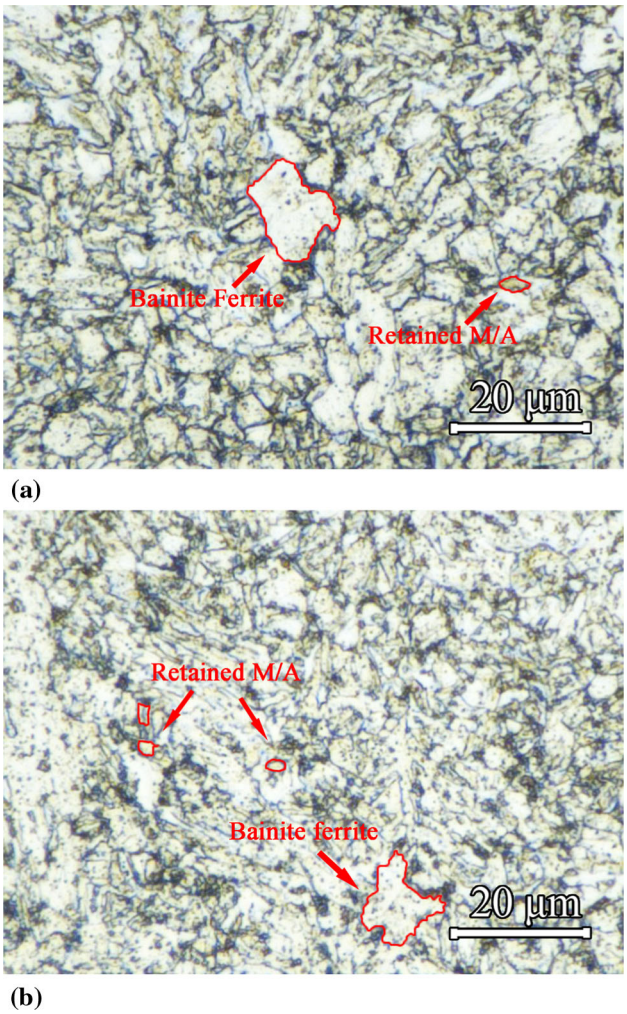

Fig. 5 Optical microstructure of 2.25Cr-1Mo-0.25V: (a) AR sample; (b) AF sample

one can identify both coarse Cr-Mn-rich carbides and V-Mo-rich fine carbides. For AF samples shown in Fig. 8(b), more Cr-Mn carbides can be found. The element analysis in AF sample shows a decrease in alloy elements dissolved in ferrite matrix and an increase in balanced Fe element compared with that in AR sample, which indicates that the ferrite grain of 2.25Cr-1Mo-0.25V has been purified after HBP. Besides, as is shown in Fig. 9(a), dislocations are seldom to be found in AR sample, whereas in AF sample shown in Fig. 9(b), one can find many HBP-induced residual dislocations.

Figure 10 shows the fracture morphology of the samples. It is easy to conclude that all the samples exhibit typical ductile rupture. All the fracture surfaces are characterized by the rough morphology with voids and dimples. Inconspicuous differences between samples with or without hydrogen damage could be noticed. These results indicate that under the present experimental condition, the failure of 2.25Cr-1Mo-0.25V steel is dominated by ductile rupture. Nevertheless, it is found that there exist smooth facets near the edge of hydrogen-involved samples' fracture surface, as is shown in Fig. 10(c)-(f). The dimension of these facets is approximated as 10-15 μm, matching with the grain size of the material.

4. Discussions

4.1 HBP-Induced Mechanical Properties and Microstructure Evolution

From the present experimental results, one can learn that the high-temperature mechanical properties of 2.25Cr-1Mo-0.25V steel suffered softening after HBP at 650 °C, which could be attributed to the evolution of microstructure during HBP (Ref 4). The microstructure evolution induced by tempering is one of the driving forces of HBP residual influence. The retained M/A phase in Fig. 4(a) indicates that the AR material was not tempered sufficiently; therefore, the material will suffer further tempering during HBP at 650 °C. According to the work of Luo et al. (Ref 7), the retained M/A phase in bainitic steel decomposed during tempering. The decomposition of hard M/A phase reduces the precipitating strengthening in the matrix, leading to the softening of material. Zhang et al. (Ref 5) reported that the fine carbides in 2.25Cr-1Mo-0.25V steel tended to transform into coarse carbides through carbide reactions and Ostwald mechanism. Jiang et al. (Ref 11) concluded that the coarsening of carbides in 2.25Cr-1Mo-0.25V steel during tempering reduced the dispersion strengthening in the matrix. What is more, both the coarsening and precipitation of carbide would consume the alloy elements in the solid solution, which reduces the solution strengthening. The reduction in alloy elements in the solution of AF samples can be verified by the EDS results shown in Fig. 8. The material degradation due to the precipitation of coarse carbides was reported by Cheruvu (Ref 12) for CrMoV rotor steel after 20000 h servicing at temperature greater than 454 °C, which exhibited a significant material softening due to the depletion of dissolved alloying elements. In Fig. 2 the strength of AF samples is lower than the strength of AFC samples, which could be induced by the inhomogeneous carbide distribution in the cylindrical ring. As is shown in Fig. 7, AF samples process more carbides that AFC samples after HBP, which would reduce the second phase strengthening and solution strengthening in the matrix, resulting in more softening of AF samples.

Only tempering effect cannot induce the inhomogeneous softening as is shown in Fig. 2. The plastic deformation could be the other driving force of carbide evolution. Arruabarrena

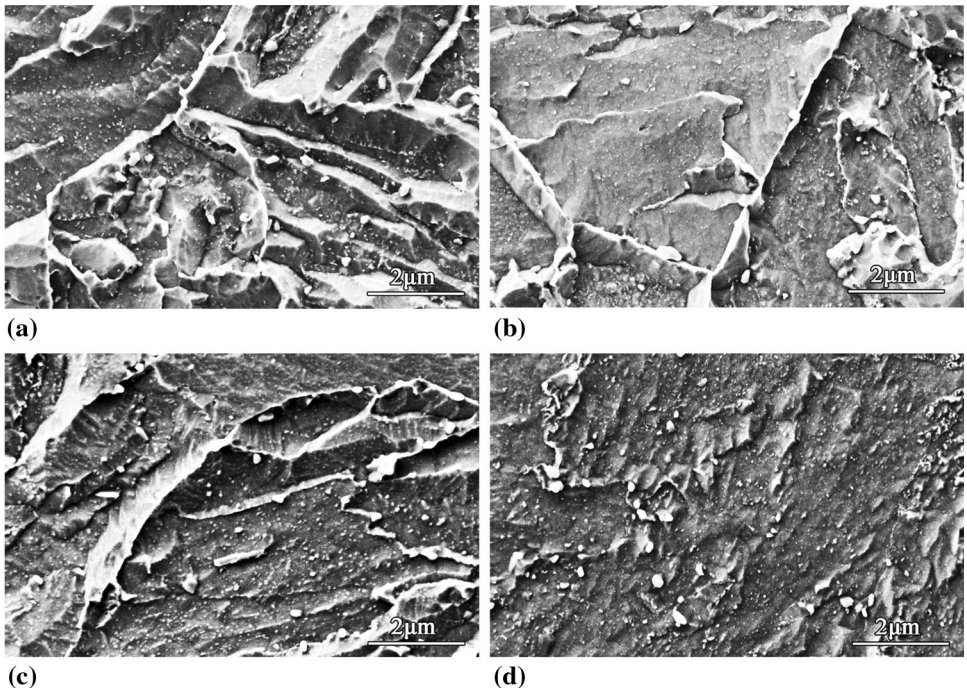

Fig. 6 Carbides in 2.25Cr-1Mo-0.25V steel: (a) AR × 10,000; (b) ARC × 10,000; (c) AF × 10,000; (d) AFC × 10,000

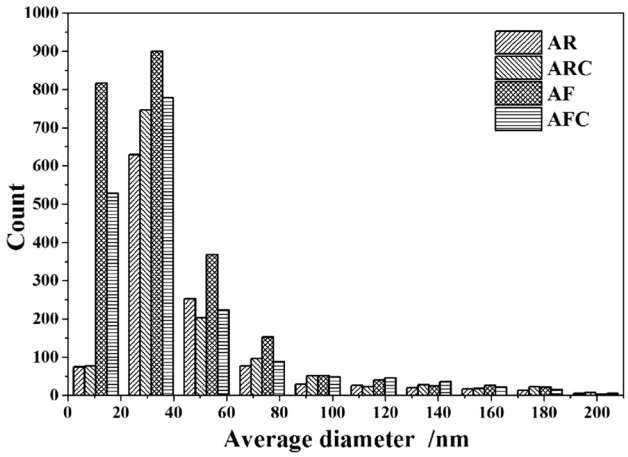

Fig. 7 Statistical results of carbides in 2.25Cr-1Mo-0.25V

et al. (Ref 13) reported that warm deformation promoted the carbide spheroidization during annealing in AISI 5140 steel. They suggested that dislocations contributed to the pipe diffusion of second phase particles and therefore enhanced local carbide coarsening. Dutta et al. (Ref 14) suggested that carbides are more prone to precipitate on dislocation sites. They proposed an mathematical model for strain-induced precipitation in Nb microalloyed steels, where carbide nucleation on dislocation mechanism was suggested to describe the strain-induced carbide evolution. Wang et al. (Ref 4) reported that the strength of 2.25Cr-1Mo-0.25V steel decreased and the density of carbides increased after high-temperature plastic deformation. According to these evidences, carbide evolution in 2.25Cr-1Mo-0.25V steel can be considered to be promoted by plastic deformation provided by HBP.

The recovery of deformed matrix is generally believed as the reason of tempering softening (Ref 15). The annihilation of dislocations and other defects during recovery contributes to the softening of matrix. However, according to Fig. 9, dislocation density in AF samples is higher than that in AR samples, which means recovery cannot annihilate all the dislocations provided by HBP. Therefore, the recovery could not be a contributor of HBP residual influence.

Based on the aforementioned discussions, we can explain the microstructure and mechanical properties evolution during HBP as following. The high temperature of HBP triggered the decomposition of retained M/A phase as well as carbide precipitating and coarsening. Meanwhile, the dislocations resulting from bending facilitate second phase particle diffusion and carbide nucleation, which promotes carbide precipitating and coarsening further. As a result, the coarsening of carbides reduced the plasticity resistance in matrix. What is more, enhanced carbide evolution consumed the dissolved strengthening phase in matrix, resulting in the degradation of ferrite matrix. The synergistic action of high-temperature tempering and plastic deformation should be responsible for the softening of the material after HBP.

4.2 Hydrogen Damage of 2.25Cr-1Mo-0.25V Steel at High Temperature

Figure 2(a) demonstrates that the strength of raw 2.25Cr-1Mo-0.25V steel is insusceptible to hydrogen while the strength of AF material increased in hydrogen environment. It is also indicated that the strengthening is positively correlated with the hydrogen concentration in material. Therefore, the material strengthening is attributed to the dissolution of gaseous hydrogen in metal. Various models and mechanisms about hydrogen-induced softening or hardening were summarized by Nagumo (Ref 16), where hydrogen in solution is generally considered as the intervener of defect interactions.

Hydrogen damage manifested as ductility loss is observed in Fig. 2(b). Hydrogen attack (HA) which deteriorates material

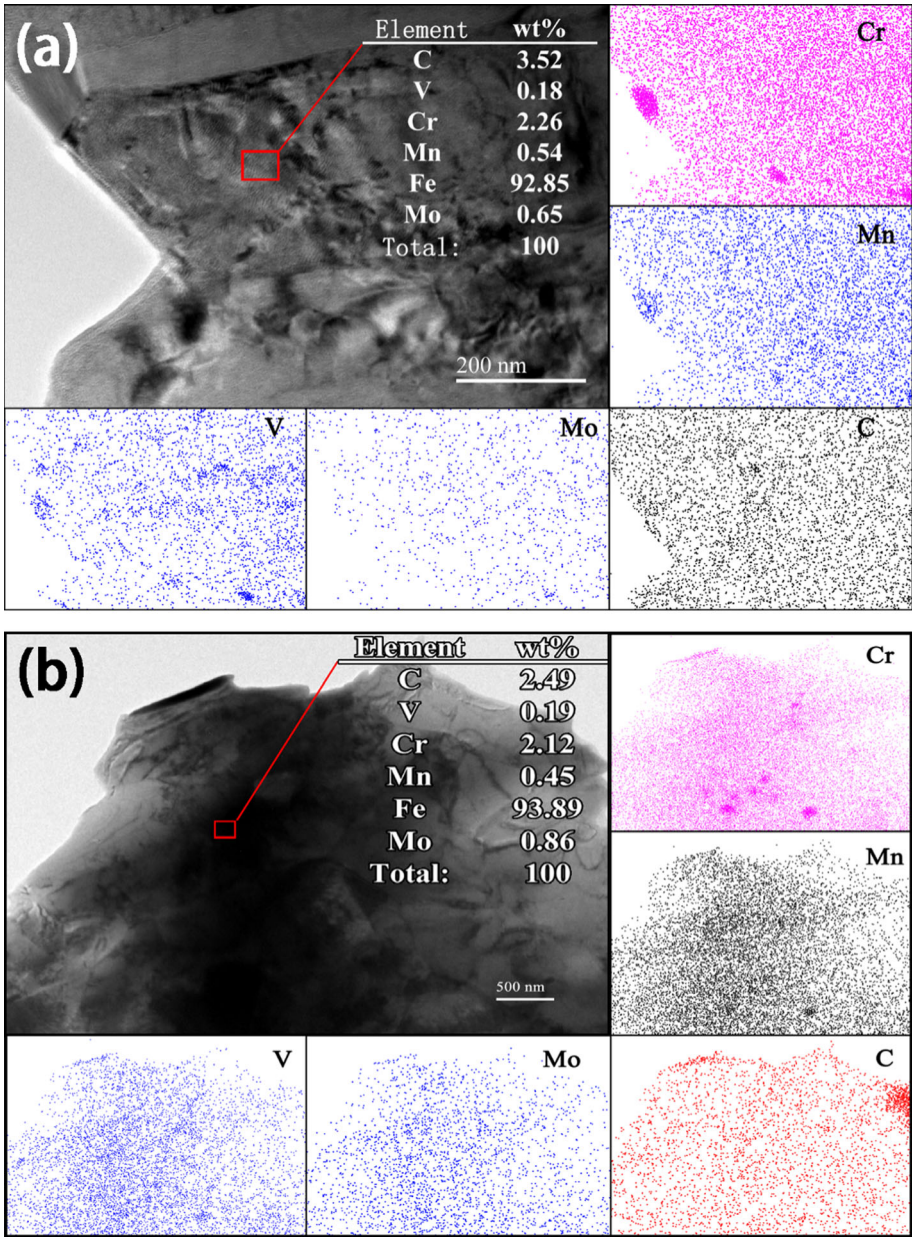

Fig. 8 TEM images and EDS results of the samples: (a) AR material; (b) AF material

through local decarburization and the formation of methane bubbles (Ref 17) is usually considered to be the primary culprit of hydrogen damage under elevated temperature. However, Nelson curve in Code API RP 941 (Ref 9) shows that under the present experimental condition, i.e., 510 °C + 1 MPa hydrogen partial pressure, 2.25Cr-1Mo-0.25V steel is allowable. Therefore, the high-temperature hydrogen damage observed in the present work is not HA. This type of high-temperature hydrogen damage (or high-temperature hydrogen embrittlement) has been found for EUROFER 97 and ODS-EUROFER steels in high-temperature hydrogen environment (Ref 10). It was concluded that hydrogen-enhanced vacancy formation at high temperature is the mechanism of hydrogen damage. Li et al. (Ref 18) investigated hydrogen's effect on the integrity of aluminum–oxide interface at high temperature, and it was suggested that hydrogen-enhanced voids nucleation and coalescence is the reason of hydrogen damage. Based on these evidences, hydrogen-induced ductility loss observed in the present work should be attributed to the interaction between hydrogen atoms and lattice defects, such as vacancies, dislocations and boundaries.

Dislocation can act as the reversible trap as well as fast transportation tunnel of hydrogen atoms (Ref 19), which implies that hydrogen concentration in metal can be increased with the propagation of dislocation. Robertson (Ref 20) studied hydrogen's influence on dislocation by deformation test of 310 s stainless steel and in situ TEM. The results proved that hydrogen can enhance the mobility of dislocations. In hydrogen-enhanced localized plasticity (HELP) mechanism (Ref 21, 22) for room temperature hydrogen embrittlement, hydrogen in solution is considered to promote localized plasticity by enhancing dislocation motions. Defect acting agent (DEFACTANT) (Ref 23) mechanism for hydrogen-related failure suggests that solution hydrogen in metal can reduce the

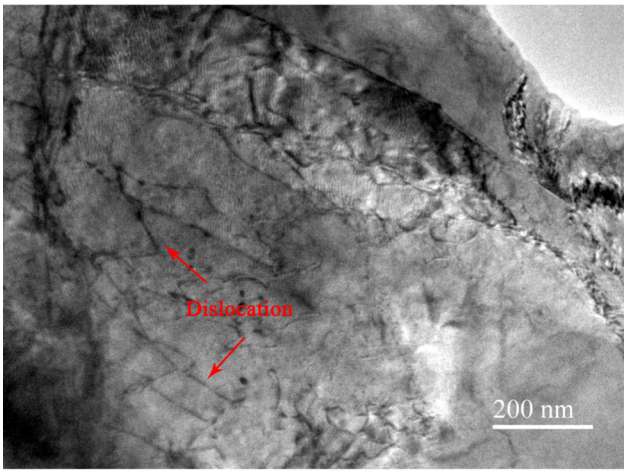

(a)

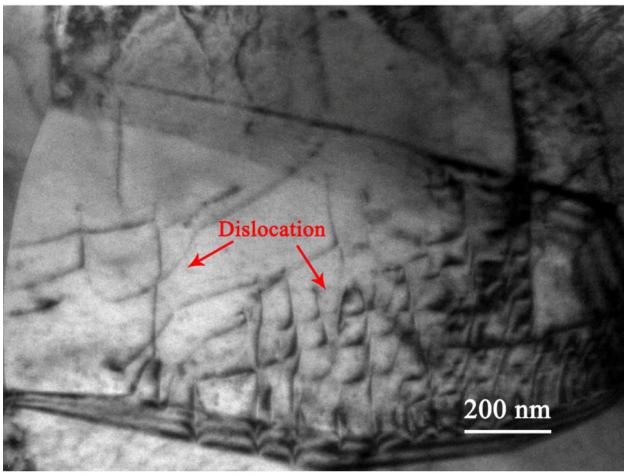

(b)

Fig. 9 Dislocations in matrix: (a) AR material; (b) AF material

formation energy of dislocation, which promotes the formation of dislocation and enhances dislocation motion. Another supporter of hydrogen-induced dislocation activity is the work of Leyson et al. (Ref 24). They studied hydrogen's effect on the onset of homogeneous dislocation nucleation (HDN) by means of multiscale approach. The simulation results indicated that hydrogen concentrations reduced HDN energy barriers significantly and thus largely enhanced dislocation plasticity. Barnoush and Vehoff (Ref 25) investigated the effect of hydrogen on dislocation nucleation using in situ electrochemical nanoindentation approach. The results manifested that hydrogen reduces the threshold for the onset of HDN by reducing the shear modulus, dislocation line energy and stacking fault energy. It was then concluded that hydrogen-induced defect formation energy is responsible for hydrogen embrittlement. Based on these evidences, in the present work, hydrogen can be considered as a "catalyst" to dislocation plasticity.

The evolution of vacancies and microvoids dominates the ductile rupture at high temperature. The role of vacancy in hydrogen-related failure was reported by Nagumo et al. (Ref 26). They studied hydrogen embrittlement of martensitic steels by a delayed fracture test and hydrogen thermal desorption analysis (TDA). The results manifested that hydrogen embrittlement susceptibility was increased by loading concurrent with hydrogen charging compared with pre-loading without hydrogen. It was suggested that hydrogen-enhanced vacancy generation plays an important role in hydrogen embrittlement. Then, Nagumo (Ref 27) proposed hydrogen-enhanced strain-induced vacancy (HESIV) theory, stating that hydrogen-enhanced vacancy formation instead of hydrogen atom itself is the nature of hydrogen embrittlement. Li et al. (Ref 28) studied the interaction between dislocations, hydrogen and vacancy by means of molecular dynamics simulation. The simulation results indicated that hydrogen atoms in solution can stabilize the vacancies in α-Fe by forming stable hydrogen–vacancy complexes, which promotes the nucleation and coalescence of microvoids. Consequentially, hydrogen-enhanced microvoids evolution would promote the ductile damage accumulation. In the present experiment, hydrogen atoms were supplied nearly infinitely from environment to the samples as they were immersed into hydrogen atmosphere. Then, the accumulation of vacancies and microvoids could be enhanced by the formation of hydrogen–vacancy complexes, which would accelerate the evolution of ductile damage. As a result, the hydrogen-enhanced damage evolution would lead to the rupture under lower true stress and macroscopic deformation, i.e., hydrogen-induced ductility loss.

In Fig. 10(c)-(f), one can identify facets in the boundary region of fracture surfaces. The average size of these facets coincides with the grain size displayed in Fig. 5(a). The facets could be induced by the loss of grain boundary cohesion as a result of high hydrogen concentration in the vicinity of sample's subsurface. Hydrogen-induced decohesion (HID) mechanism (Ref 29) could explain the formation of these facets. High hydrogen concentration in subsurface would promote the evolution of vacancies and dislocations. Then, the defects stacked at grain boundaries would reduce the cohesion between boundaries. As a result, intergranular cracking would take place on some grains, leading to a suddenly rupture. HID would lower the threshold stress for unstable microcrack propagation, leading to the rupture under lower macroscopic plastic deformation.

As is discussed in this section, it is suggested that the synergistic action of hydrogen-enhanced dislocation activity and hydrogen-enhanced vacancy evolution is responsible for the hydrogen-induced ductility loss. It should be warned that in the present work, the material degradation caused by high-temperature hydrogen is confined by the present experimental condition. However, there is still a potential that the material might be poisoned by hydrogen more serious if hydrogen concentration in material increases further.

4.3 HBP Residual Influence on the High-Temperature Hydrogen Damage

The experimental results demonstrated that HBP enhanced the hydrogen damage susceptibility of 2.25Cr-1Mo-0.25V steel at high temperature. Based on the aforementioned discussions on microstructure evolution and hydrogen damage mechanism, the impact of HBP on the hydrogen damage could be explained as follows.

4.3.1 HBP-Enhanced Diffusible Hydrogen Concentration. As is discussed in section 4.1, the carbide in 2.25Cr-1Mo-0.25V tended to precipitating and coarsening during HBP. According to the hydrogen TDA on AISI 4340 (Ref 30), the binding energy of carbide-type hydrogen trap is 72 kJ/mol which is higher than that of dislocation (18 kJ/mol) and grain boundary (48 kJ/mol). Takai and Watanuki (Ref 31) concluded

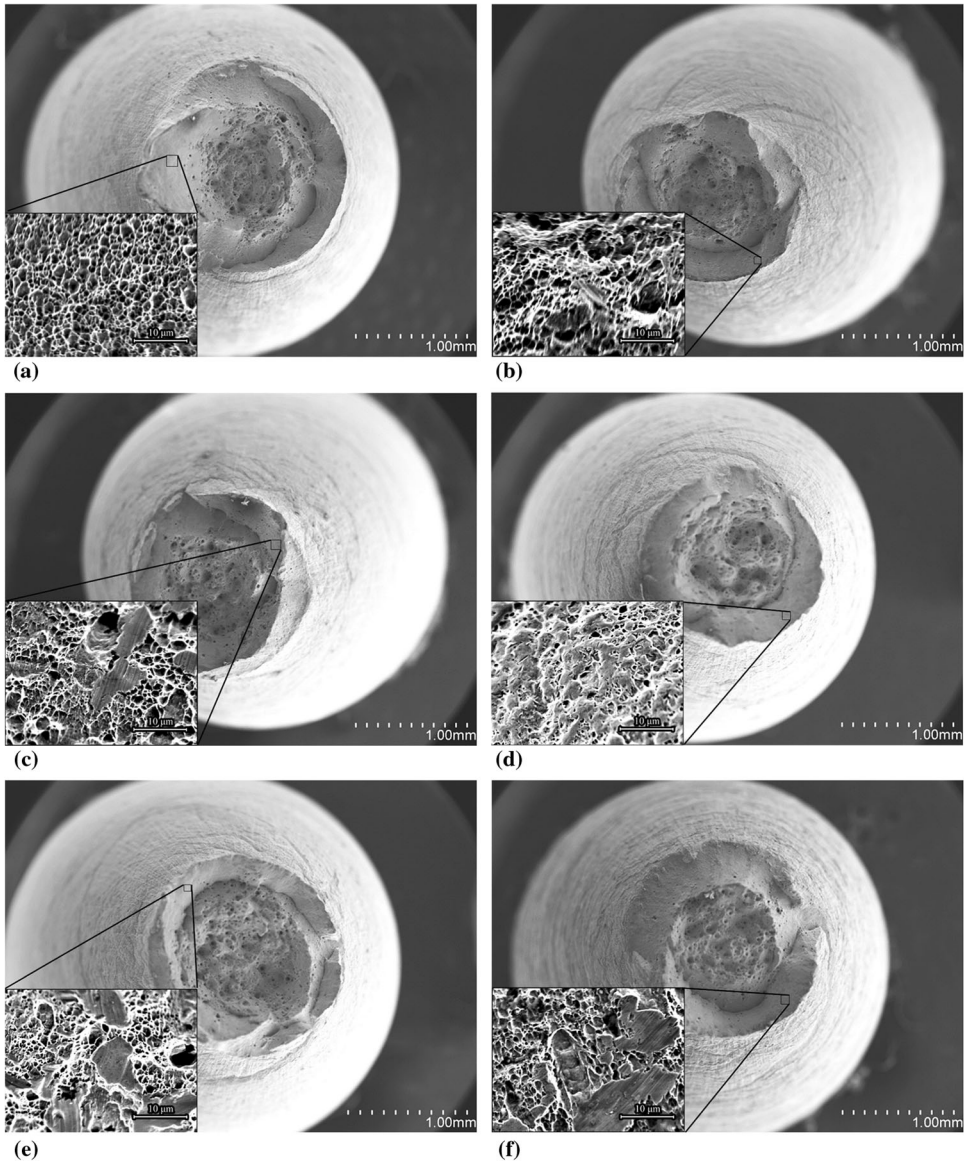

Fig. 10 Fracture microstructure of the samples: (a) AR-Ar; (b) AF-Ar; (c) AR-H2; (d) AF-H2; (e) AR-H2-24; (f) AF-H2-24

that the strongly trapped hydrogen with binding energy of 65.0 kJ/mol is innocuous to the environmental hydrogen embrittlement of high-strength steels. Therefore, carbide-type hydrogen trap is considered to be innocent with hydrogen damage of 2.25Cr-1Mo-0.25V steel at room temperature. However, hydrogen atoms bonded in carbide traps could overcome the potential barrier of its trap to become diffusible once given sufficient energy input. The activation of trapped hydrogen in carbide traps under elevated temperature has been verified by the TDA on CrMo steel (Ref 32), which reported a second desorption peak for carbide traps at about 500 °C. This phenomenon implies that the increase in carbide density induced by HBP could provide more available hydrogen atoms to 2.25Cr-1Mo-0.25V steel when tested under 510 °C. On the other hand, the residual dislocation density induced by HBP is confirmed in Fig. 9(b), which would also provide reversible hydrogen traps and contribute to the hydrogen accumulation in material. Accordingly, the effect of HBP on the diffusible hydrogen concentration can be explained by the mechanism shown in Fig. 11(a). As is shown in Fig. 11(a), HBP-induced microstructure evolution resulted in more carbides and dislocations in 2.25Cr-1Mo-0.25V steel, which would provide more reversible hydrogen traps under elevated temperature. Consequentially, AF material would sustain more diffusible hydrogen atoms than AR material, enhancing the effect of hydrogen on the material.

4.3.2 HBP-Enhanced Ductile Damage Evolution. It has been suggested that HPB residual influence reduced both the second phase strengthening and solution strengthening, which reduces the dislocation plasticity resistance in 2.25Cr-1Mo-0.25V matrix. Therefore, dislocation propagation would be easier and hydrogen's effect on dislocation motion would be more significant in AF material. Figure 11(b) illustrates a possible mechanism for the ductile damage evolution in

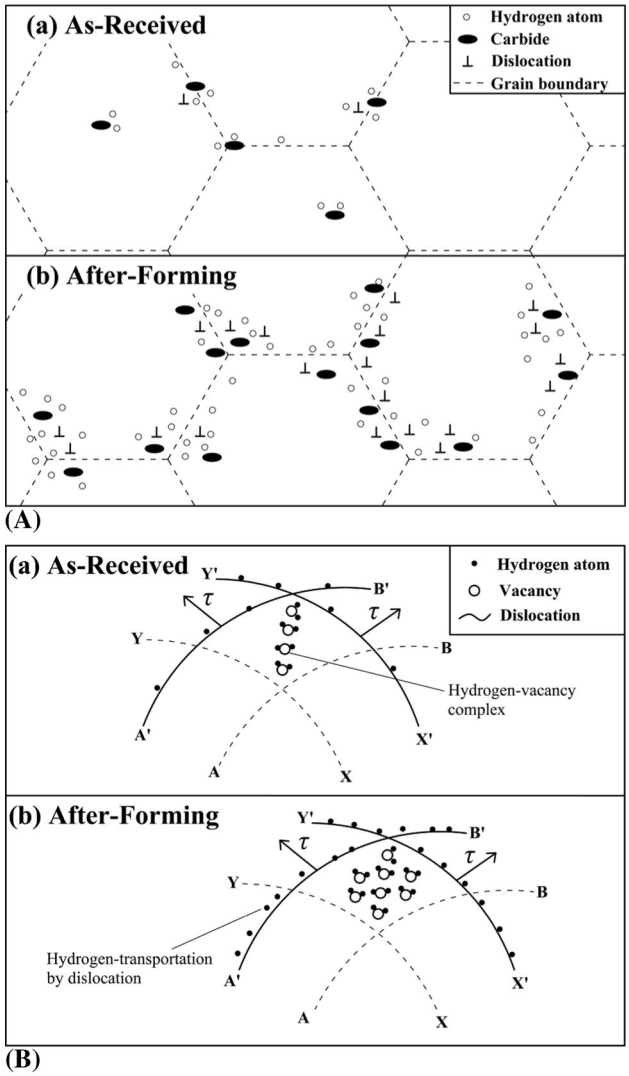

Fig. 11 Illustration of the impact of HBP on the hydrogen damage of 2.25Cr-1Mo-0.25V at high temperature: (a) enhanced hydrogen concentration; (b) enhanced hydrogen damage evolution

2.25Cr-1Mo-0.25V steel during the SSRT test in high-temperature hydrogen environment. For AF sample which has been degenerated by HBP, the synergistic action of both the increased hydrogen concentration and decreased dislocation motion resistance would promote the vacancy formation and clustering. As is shown in Fig. 11(b), when dislocation intersection takes place (dislocation AB moves to A'B', while XY moves to X'Y'), higher diffusible hydrogen concentration in AF material would stabilize more vacancies by forming hydrogen–vacancy complexes. Meanwhile, the effect of purified ferrite matrix superposing on the effect of hydrogen-enhanced dislocation motion would increase the dislocation motion impetus τ in AF material, which would accelerate the clustering of vacancies to facilitate microvoids nucleation and coalescence. Eventually, the accelerated ductile damage evolution would breed the rupture under lower deformation and true stress, observed as more hydrogen-induced ductility loss in AF material. This mechanism could explain the impact of HBP on the high-temperature hydrogen damage of 2.25Cr-1Mo-0.25V steel. The stress–strain curve in Fig. 4(b) shows that in the plastic damage accumulation process, AF-H2-24 sample presents the most pronounced damage accumulation speed compared with AF-H2 and AF-Ar samples, which supports the rationality of the proposed mechanism.

5. Conclusions

In the present work, the SSRT test of 2.25Cr-1Mo-0.25V steel with or without the residual influence of hot bending process was conducted in 1 MPa hydrogen atmosphere at 510 °C. The impact of hot bending process on the high-temperature mechanical properties and hydrogen damage of 2.25Cr-1Mo-0.25V steel was studied. The experimental results were discussed with respect to the evolution of microstructure, the mechanism of high-temperature hydrogen damage and the impact of hot bending process on the hydrogen damage. Some conclusions can be drawn:

1. 2.25Cr-1Mo-0.25V steel was softened after hot bending process. The degradation of mechanical properties was attributed to the reduction in second phase strengthening and solution strengthening resulting from the coarsening and precipitation of carbides during the synergistic action of high-temperature tempering and plastic deformation.
2. High-temperature hydrogen damage can induce the ductility loss of 2.25Cr-1Mo-0.25V steel, mainly manifested as the reduction in elongation in high-temperature hydrogen environment.
3. 2.25Cr-1Mo-0.25V steel with hot bending residual influence is more susceptible by high-temperature hydrogen damage than its virgin state. The impact of hot bending process on the hydrogen damage susceptibility of 2.25Cr-1Mo-0.25V steel could be attributed to the evolution of microstructure during high-temperature plastic deformation. Both the increase in hydrogen uptake capacity owing to carbide evolution and the reduction in dislocation plasticity resistance caused by material softening would accelerate the evolution of ductile damage during loading in hydrogen environment, resulting in the increase in hydrogen damage susceptibility after the material was hot-bended.

Acknowledgment

This work was supported by National Key Basic Research and Development Project of China (973 Project, No. 2015CB057603).

References

1. A.E. Tekkaya, J.M. Allwood, P.F. Bariani, S. Bruschi, J. Cao, S. Gramlich, P. Groche, G. Hirt, T. Ishikawa, and C. Löbbe, Metal Forming Beyond Shaping: Predicting and Setting Product Properties, *CIRP Ann. Manuf. Technol.*, 2015, **64**(2), p 629–653
2. D. Zeng, S.D. Liu, V. Makam, S. Shetty, L. Zhang, and F. Zweng, Specifying Steel Properties and Incorporating Forming Effects in Full Vehicle Impact Simulation. In: *SAE 2002 World Congress & Exhibition* 2002
3. A.-M. Brass, F. Guillon, and S. Vivet, Quantification of Hydrogen Diffusion and Trapping in 2.25Cr-1Mo and 3Cr-1Mo-V Steels with the

Electrochemical Permeation Technique and Melt Extractions, *Metall. Mater. Trans. A*, 2004, **35**(5), p 1449–1464
4. Y. Wang, G. Cheng, M. Qin, Q. Li, Z. Zhang, K. Chen, Y. Li, H. Hu, W. Wu, and J. Zhang, Effect of High Temperature Deformation on the Microstructure, Mechanical Properties and Hydrogen Embrittlement of 2.25Cr-1Mo-0.25V Steel, *Int. J. Hydrogen Energy*, 2017, **42**(38), p 24549–24559
5. Y. Zhang, L. Miao, X. Wang, H. Zhang, and J. Li, Evolution Behavior of Carbides in 2.25Cr1Mo0.25V Steel, *Mater. Trans.*, 2009, **50**(11), p 2507–2511
6. Z. Jiang, P. Wang, D. Li, and Y. Li, Effects of Tempering Temperature on the Microstructure and Mechanical Properties of Granular Bainite in 2.25 Cr-1Mo-0.25V Steel, *Acta Metall. Sin.*, 2015, **51**(8), p 925–934
7. Y. Luo, J.M. Peng, H.-B. Wang, and X.-C. Wu, Effect of Tempering on Microstructure and Mechanical Properties of a Non-Quenched Bainitic Steel, *Mater. Sci. Eng., A*, 2010, **527**(15), p 3433–3437
8. X.L. Liu, X.D. Chen, B. Wang, Z.C. Fan, and Q.W. Zhuang, Development of New Material Testing Apparatus in Hydrogen at Elevated Temperature, *Proced. Eng.*, 2015, **130**, p 1046–1056
9. RP941 A, *Steels for Hydrogen Service at Elevated Temperatures and Pressures in Petroleum Refineries and Petrochemical Plants*, API, Publishing Services, Washington, DC, 2016
10. E. Malitckii, Y. Yagodzinskyy, and H. Hänninen, Hydrogen-Induced Crack Nucleation in Tensile Testing of EUROFER 97 and ODS-EUROFER Steels at Elevated Temperature, *J. Nucl. Mater.*, 2015, **466**, p 286–291
11. Z. Jiang, P. Wang, D. Li, and Y. Li, The Evolutions of Microstructure and Mechanical Properties of 2.25Cr-1Mo-0.25V Steel with Different Initial Microstructures During Tempering, *Mater. Sci. Eng., A*, 2017, **699**, p 165–175
12. N.S. Cheruvu, Degradation of Mechanical Properties of Cr-Mo-V and 2.25Cr-1Mo Steel Components After Long-Term Service at Elevated Temperatures, *Metall. Trans. A*, 1989, **20**(1), p 87–97
13. J. Arruabarrena, B. López, and J.M. Rodriguez-Ibabe, Influence of Prior Warm Deformation on Cementite Spheroidization Process in a Low-Alloy Medium Carbon Steel, *Metall. Mater. Trans. A*, 2014, **45**(3), p 1470–1484
14. B. Dutta, E.J. Palmiere, and C.M. Sellars, Modelling the Kinetics of Strain Induced Precipitation in Nb Microalloyed Steels, *Acta Mater.*, 2001, **49**(5), p 785–794
15. L. Storojeva, D. Ponge, R. Kaspar, and D. Raabe, Development of Microstructure and Texture of Medium Carbon Steel During Heavy Warm Deformation, *Acta Mater.*, 2004, **52**(8), p 2209–2220
16. Nagumo M (2016) Deformation Behaviors. In: *Fundamentals of Hydrogen Embrittlement*. Springer, Berlin, pp. 79–101
17. M. Martin, M. Dadfarnia, S. Orwig, D. Moore, and P. Sofronis, A Microstructure-Based Mechanism of Cracking in High Temperature Hydrogen Attack, *Acta Mater.*, 2017, **140**, p 300–304
18. M. Li, D.G. Xie, E. Ma, J. Li, X.X. Zhang, and Z.W. Shan, Effect of Hydrogen on the Integrity of Aluminium-Oxide Interface at Elevated Temperatures, *Nat. Commun.*, 2017, **8**, p 14564
19. M. Dadfarnia, M.L. Martin, A. Nagao, P. Sofronis, and I.M. Robertson, Modeling Hydrogen Transport by Dislocations, *J. Mech. Phys. Solids*, 2015, **78**, p 511–525
20. I. Robertson, The Effect of Hydrogen on Dislocation Dynamics, *Eng. Fract. Mech.*, 2001, **68**(6), p 671–692
21. Sofronis Pt, Y. Liang, and N. Aravas, Hydrogen Induced Shear Localization of the Plastic Flow in Metals and Alloys, *Eur. J. Mech. A/Solids*, 2001, **20**(6), p 857–872
22. Y. Liang, P. Sofronis, and N. Aravas, On the Effect of Hydrogen on Plastic Instabilities in Metals, *Acta Mater.*, 2003, **51**(9), p 2717–2730
23. R. Kirchheim, On the Solute-Defect Interaction in the Framework of a Defactant Concept, *Int. J. Mater. Res.*, 2009, **100**(4), p 483–487. https://doi.org/10.3139/146.110065
24. G.P.M. Leyson, B. Grabowski, and J. Neugebauer, Multiscale Modeling of Hydrogen Enhanced Homogeneous Dislocation Nucleation, *Acta Mater.*, 2016, **107**, p 144–151
25. A. Barnoush and H. Vehoff, Recent Developments in the Study of Hydrogen Embrittlement: Hydrogen Effect on Dislocation Nucleation, *Acta Mater.*, 2010, **58**(16), p 5274–5285
26. M. Nagumo, M. Nakamura, and K. Takai, Hydrogen Thermal Desorption Relevant to Delayed-Fracture Susceptibility of High-Strength Steels, *Metall. Mater. Trans. A*, 2001, **32**(2), p 339–347
27. M. Nagumo, Hydrogen Related Failure of Steels—A New Aspect, *Mater. Sci. Technol.*, 2004, **20**(8), p 940–950
28. S. Li, Y. Li, Y.C. Lo, T. Neeraj, R. Srinivasan, X. Ding, J. Sun, L. Qi, P. Gumbsch, and J. Li, The Interaction of Dislocations and Hydrogen-Vacancy Complexes and Its Importance for Deformation-Induced Proto Nano-Voids Formation in α-Fe, *Int. J. Plast*, 2015, **74**, p 175–191
29. Nagumo M (2016) Mechanistic Aspects of Fracture II ∼ Plasticity-Dominated Fracture Models. In: *Fundamentals of Hydrogen Embrittlement*. Springer, Berlin, pp. 217-239
30. P. Novak, R. Yuan, B. Somerday, P. Sofronis, and R. Ritchie, A Statistical, Physical-Based, Micro-Mechanical Model of Hydrogen-Induced Intergranular Fracture in Steel, *J. Mech. Phys. Solids*, 2010, **58**(2), p 206–226
31. K. Takai and R. Watanuki, Hydrogen in Trapping States Innocuous to Environmental Degradation of High-strength Steels, *ISIJ Int.*, 2003, **43**(4), p 520–526
32. H.J. Kang, J.S. Yoo, T.P. Ji, S.T. Ahn, N. Kang, and K.M. Cho, Effect of Nano-Carbide Formation on Hydrogen-Delayed Fracture for Quenching and Tempering Steels During High-Frequency Induction Heat Treatment, *Mater. Sci. Eng., A*, 2012, **543**(5), p 6–11